Temperature Dependence of Interband Transitions in Wurtzite InP Nanowires

ARTICLE *in* ACS NANO · MARCH 2015

Impact Factor: 12.88 · DOI: 10.1021/acsnano.5b00699 · Source: PubMed

Temperature Dependence of Interband Transitions in Wurtzite InP Nanowires

Attilio Zilli,[†,§] Marta De Luca,[†] Davide Tedeschi,[†] H. Aruni Fonseka,[‡] Antonio Miriametro,[†] Hark Hoe Tan,[‡] Chennupati Jagadish,[‡] Mario Capizzi,[†] and Antonio Polimeni*[,†]

[†]Dipartimento di Fisica, Sapienza Università di Roma, P.le A. Moro 2, 00185 Roma, Italy and [‡]Department of Electronic Materials Engineering, Research School of Physics and Engineering, The Australian National University, Canberra, ACT 0200, Australia [§]Present address: School of Biosciences, Cardiff University, The Sir Martin Evans Building, Museum Avenue, Cardiff CF10 3AX, Wales, United Kingdom.

ABSTRACT Semiconductor nanowires (NWs) formed by non-nitride III–V compounds grow preferentially with wurtzite (WZ) lattice. This is contrary to bulk and two-dimensional layers of the same compounds, where only zincblende (ZB) is observed. The absorption spectrum of WZ materials differs largely from their ZB counterparts and shows three transitions, referred to as A, B, and C in order of increasing energy, involving the minimum of the conduction band and different critical points of the valence band. In this work, we determine the temperature dependence (T = 10–310 K) of the energy of transitions A, B, and C in ensembles of WZ InP NWs by photoluminescence (PL) and PL excitation (PLE) spectroscopy. For the whole temperature and energy ranges investigated, the PL and PLE spectra are quantitatively reproduced by a theoretical model taking into account contribution from both exciton and continuum states. WZ InP is found to behave very similarly to wide band gap III-nitrides and II–VI compounds, where the energy of A, B, and C displays the same temperature dependence. This finding unveils a general feature of the thermal properties of WZ materials that holds regardless of the bond polarity and energy gap of the crystal. Furthermore, no differences are observed in the temperature dependence of the fundamental band gap energy in WZ InP NWs and ZB InP (both NWs and bulk). This result points to a negligible role played by the WZ/ZB differences in determining the deformation potentials and the extent of the electron–phonon interaction that is a direct consequence of the similar nearest neighbor arrangement in the two lattices.

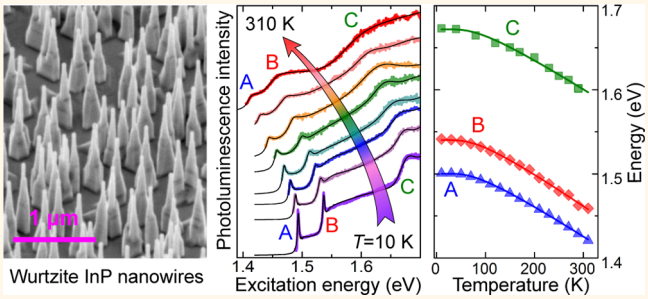

KEYWORDS: InP nanowires · wurtzite and zincblende structures · band-structure critical points · thermal properties · photoluminescence excitation spectroscopy

Semiconductor nanowires (NWs) are regarded as versatile building blocks for nanoelectronics, nanophotonics, biosensing, and solar cell devices.[1] They are usually obtained by the vapor–liquid–solid growth mode, are typically a few microns long, and have a diameter ranging between a few and a few hundreds of nanometers. Most of the interesting and useful properties of NWs stem from their large surface-to-volume ratio, which is also one of the factors leading to the existence of NWs with crystal phases not observable in bulk and two-dimensional layers.[2] This is the case of NWs formed by III-(As,P) compounds, such as InP, GaAs, InAs, and GaP, that may grow with either wurtzite (WZ) or zincblende (ZB) lattice. Often WZ and ZB lattices coexist within a same wire[3] offering the unprecedented possibility to modulate the physical properties of the NWs along their axis without varying the material composition.[4] Indeed, WZ and ZB lattices differ largely in many band structure parameters, such as band gap energy (E_g),[5–8] critical point symmetries,[9–12] carrier effective mass and gyromagnetic factor,[13,14] *etc.* Furthermore, the two phases feature a quite diverse valence-band (VB) structure as a result of the lower crystal point symmetry of WZ that produces a crystal field perturbation. The latter combines with the spin–orbit interaction leading to three VB states with Γ_9^V, Γ_{7u}^V, and Γ_{7l}^V symmetries at $k = 0$ in order of increasing hole energy.[5,9–11,15,16] Transitions between these VB states and the bottommost conduction band (CB) minimum, with Γ_7^C or Γ_8^C symmetry (still an open issue in GaAs NWs; see ref 11 for a review) result in three different absorption/emission

* Address correspondence to antonio.polimeni@roma1.infn.it.

Received for review January 30, 2015 and accepted March 23, 2015.

Published online 10.1021/acsnano.5b00699

bands referred to as A, B, and C for increasing photon energy. Following refs 17 and 18, we associate to each of these transitions an energy gap $E_{g,i}$ with i = A, B, and C, $E_{g,A}$ being the fundamental band gap energy of the crystal.

Depending on the crystal phase and transition considered, one may also expect a different response of the electronic properties to external perturbations such as stress, magnetic field, and temperature (T). In particular, the variation of E_g with T provides valuable information on the lattice thermal expansion and the extent of the electron−phonon interaction.[17,19] Indeed, a different band symmetry might affect the strength of the electron−phonon interaction and thus lead to a different temperature dependence of the band gap energy. For instance, a variation of the PL peak energy with T different from that observed in ZB bulk GaAs was reported in WZ GaAs NWs and ascribed to a Γ_8^C symmetry of the WZ CB minimum.[20] A Γ_7^C symmetry has been instead proposed by the same authors in ref 21. In addition, T-dependent optical studies hold a great importance with regard to potential applications of nanowires for room-temperature operation, such as in photodetectors and solar cells. In that context, the absorption spectrum and the experimental conditions favoring an efficient light-to-charge carriers conversion is pivotal for assessing the suitability of NWs made of a specific material.

The temperature dependence of the fundamental energy gap in NWs has been addressed so far mainly by photoluminescence (PL) studies. Here, we focus on InP NWs, a material system whose electronic properties have been intensely investigated in recent years.[6,14,22−31] A. Mishra *et al.* first compared the temperature dependence of the PL peak energy of ZB and WZ InP NWs.[6] Both these dependences were fitted by a modified Varshni's formula

$$E(T) = E(0) - \alpha T^4/(T^3 + \beta) \quad (1)$$

where $E(0)$ is the PL peak energy at 0 K, and α and β are two adjustable parameters (in the usual Varshni's equation the T^4 and T^3 terms are replaced by T^2 and T, respectively).[19] The PL peak energy of WZ NWs was found to follow the same temperature dependence of a ZB InP epilayer, while, surprisingly, ZB NWs at high temperatures exhibited a significantly different trend. M. H. Hadj Alouane *et al.*, instead, could not fit their PL data on WZ InP nanowires by the Varshni's equation, and resorted to the relation[26]

$$E(T) = E_B - a[1 + 2/(e^{\theta/T} - 1)] \quad (2)$$

where $(E_B - a) = E(0)$ is the PL peak energy at 0 K, a roughly estimates the strength of the electron−phonon interaction and $k_B\theta$ is an average phonon energy.[32] Similarly to eq 1, eq 2 also predicts a linear behavior at high temperature.[33] A usual Varshni's dependence of the PL peak energy was reported by our group in WZ InP NWs,[14] and by K. Li *et al.* in InP nanoneedles grown on Si,[28] where no major differences were found between ZB and WZ phases, except for different $E(0)$ values.

Although PL is invaluable in most instances, low-temperature emission spectra are usually affected by defect-related localized states, which may blur the band gap free-exciton peak and distort its temperature dependence as localized carriers are progressively ionized.[34,35] Moreover, the transition from exciton to band-to-band recombination regime with increasing T can hinder the true thermal variation of the band gap,[36] while thermal broadening hampers an accurate band-gap energy determination at high temperatures.[26] Finally, PL peaks are usually red-shifted with respect to the corresponding absorption peaks by an amount referred to as Stokes shift. The extent of such a red-shift varies with temperature and depends on the interplay between disorder effects, which broaden the electronic joint density-of-states, and the thermal occupation of levels by photogenerated carriers.[37,38] All these factors, which impede an accurate estimate of the energy gap from PL measurements alone, could cause some of the aforementioned discrepancies between reports by various authors. In addition, PL hardly gives access to higher-energy transitions, such as B and C in WZ semiconductors. Indeed, so far temperature-dependent optical studies in WZ-phase NWs were restricted to the band gap transition A and did not explore B and C, but in GaAs.[7,39] In ref 39, the T dependence of C was reported but not compared with that of A and B transitions. In ref 7, we found that A and B exhibit a similar band gap thermal reduction.

In this work, we employ PL excitation (PLE) measurements from 10 to 310 K to establish the temperature dependence of the energy gaps associated with A, B, and C transitions in WZ InP NWs. A model for optical absorption taking into account excitonic as well as continuum state transitions reproduces very well the entire PLE spectrum over a 0.30 eV interval at all the investigated temperatures. Interestingly, the thermal shrinkage of A, B, and C band gap energies follows the same law, as reported in other technologically relevant WZ phase materials, such as ZnO,[17] GaN,[40] CdS,[18] and CdSe.[41] A quantitative analysis of the PL spectra recorded in a same temperature range confirms the results obtained on transition A. Useful information about the role of the crystal phase on the factors determining the band gap thermal reduction are derived by a comparison with PL measurements on ZB InP NWs and bulk.

RESULTS AND DISCUSSION

Growth and Structural Properties of the Samples. We investigated WZ-phase InP NWs grown on semi-insulating InP (111)B substrates at 480 °C with V/III ratios of 350 and 110. In the two samples, the NWs

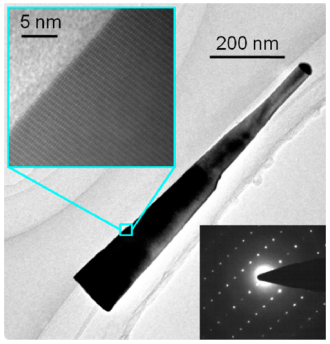

Figure 1. Transmission electron microscopy image of a typical wurtzite InP nanowire grown with a V/III ratio of 110. The top-left inset is a high-resolution image taken along the [11−20] zone axis recorded close to the wire base, as indicated by the square. This image and the diffraction pattern of the selected area (bottom-right inset) confirm the WZ crystal structure of the nanowire.

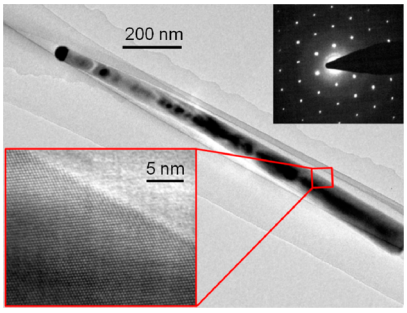

Figure 2. Transmission electron microscopy image of a typical zincblende InP nanowire. The bottom-left inset is a high-resolution image taken along the [110] zone axis. The atomic pattern indicates a ZB phase, as also demonstrated by the diffraction pattern of the selected area shown in the top-right inset.

are ∼1 μm-long, standing vertically on the substrate, and feature a tapered shape. As the two samples show very similar structural and optical properties, they will be regarded as a same sample from now on. For PLE measurements, we used the NWs grown with a V/III ratio of 350. For PL measurements, we used mainly the NWs grown with a V/III ratio of 110. A transmission electron microscopy (TEM) image of a representative nanowire of the latter sample is presented in the main part of Figure 1. Except for a very few stacking faults located at the tip of the NW, no other planar defects are found over the whole wire length. The high-resolution TEM in the top left inset highlights a pure WZ phase, with the $\hat{c}$ axis directed along the NW symmetry axis. The corresponding diffraction pattern in the bottom right inset further demonstrates the defect-free WZ structure. Similar pure WZ phase with almost no stacking faults has been found also in the NWs grown with a V/III ratio of 350; see refs 14 and 31.

ZB-phase NWs were grown on a semi-insulating InP (100) substrate at 450 °C with V/III ratio of 350. These nanowires have a square section and are slightly tapered.[42] Figure 2 shows TEM micrographs of a typical ZB NW at two magnifications and an electron diffractogram (top right inset). The ZB lattice exhibits an excellent crystalline quality with no twins or other structural defects. An InP bulk sample was also studied for comparison purposes.

Temperature-Dependent PL and PLE. In a typical PLE experiment, PL emission is recorded at a fixed detection energy, E_{det}, as a function of the excitation wavelength λ_{exc}. Under some assumptions,[43] a PL excitation spectrum is equivalent to an absorption spectrum that makes PLE very suitable for analyzing absorption mechanisms in nanostructures, where standard transmission measurements would be difficult. Low-temperature (10 K) PL and PLE spectra of an ensemble (about 3 × 10^5 NWs were probed) of WZ InP NWs grown with a V/III ratio of 350 are shown in Figure 3.

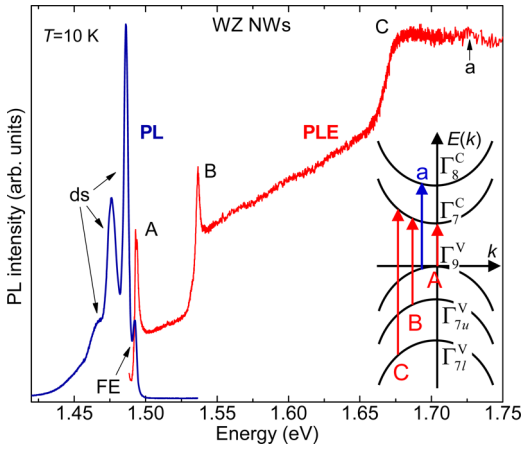

Figure 3. T = 10 K photoluminescence (PL, blue line) and PL excitation (PLE, red line) spectra of an ensemble of wurtzite InP nanowires. The PLE detection energy was 1.486 eV. PL: FE indicates the recombination line of the fundamental band gap free-exciton, "ds" refers to carrier recombination at point and line defects present in the lattice. PLE: A, B, and C, in that order, indicate the three lowest energy transitions peculiar to the WZ band structure, as shown in the inset (not in scale). "a" indicates a transition involving the second conduction band minimum Γ_8^C.

The spectra were recorded on NWs standing vertical on the substrate in a backscattering configuration, namely, with laser and PL collection directions both perpendicular to the substrate (and parallel to the WZ $\hat{c}$ axis). The PL spectrum exhibits several contributions. The highest energy peak (1.492 eV) is due to the band gap free-exciton (FE) recombination, known as A exciton in WZ semiconductors.[15−17,22,27] The low-energy features can be ascribed to point or line defect states (labeled as "ds"),[4,28,30] as suggested by their dependence on power and temperature (not shown here).[31] The PLE spectrum, obtained by setting E_{det} = 1.486 eV, shows three step-like absorption edges characteristic of the WZ band structure. These transitions involve the bottommost CB minimum, with Γ_7^C symmetry in InP,[9,11] and the three VB maxima, with Γ_9^V, Γ_{7u}^V, and Γ_{7l}^V symmetry, labeled as A, B, and C, respectively (see sketch in the inset). At T = 10 K we find that the

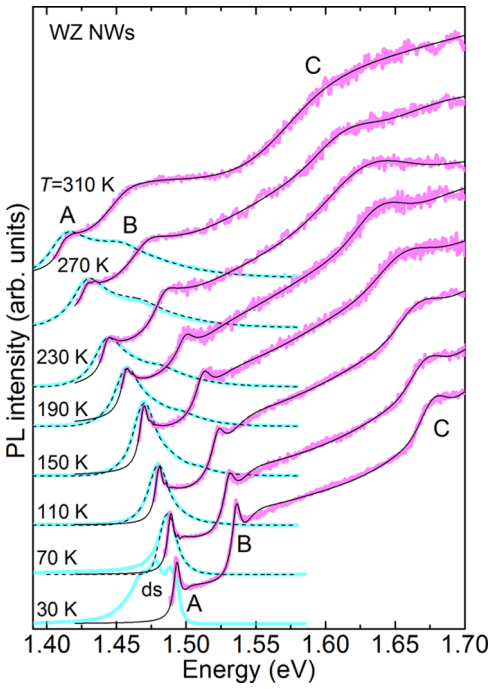

Figure 4. Photoluminescence (PL, thick cyan lines) and PL excitation (PLE, thick magenta lines) spectra recorded at different temperatures on an ensemble of wurtzite InP nanowires. PL: "ds" (bottommost spectrum) indicates carrier recombination at point and line defects present in the lattice. Thin black *dashed* lines are fits of eq 4 to the data. PLE: detection energies were set on the low-energy side of the fundamental band gap free-exciton. Thin black *solid* lines are fits of eq 3 to the data. In both PL and PLE spectra, A, B, and C indicate the three lowest energy transitions pertinent to the WZ band structure, as shown in the inset in Figure 3. In PL, B is visible only for $T > 150$ K.

resonance energies are $E_A = 1.493$ eV, $E_B = 1.537$ eV, and $E_C \sim 1.675$ eV (in the latter case the energy is estimated from the change of slope of the spectrum around C). These values are in good agreement with previous experimental results[22−24,26,27,31] and *ab initio* calculations[12] on WZ InP NWs. We notice that A and B absorption edges exhibit extremely sharp excitonic features (line width ∼2 meV). The high optical quality of the NWs is also confirmed by the small value of the Stokes shift of the fundamental transition A amounting to $(E^A_{PLE} - E^A_{PL}) = (1.493 - 1.492)$ eV = 1 meV. No evident exciton resonance is seen for C, while a tiny feature, marked as "a", is observed just above the C absorption edge. We attribute "a" to a transition involving electrons in the second CB Γ^C_8 and holes in the VB maximum Γ^V_9 (see sketch in the inset). Thus, the 232 meV energy separation of "a" from the A transition would correspond to the CB $(\Gamma^C_8 - \Gamma^C_7)$separation, in quantitative agreement with previous theoretical[9] and experimental[27] studies.

The evolution of PL and PLE spectra of WZ nanowires with temperature is shown in Figure 4. The thick colored lines represent the experimental data while the thin black lines are the results of a line shape fitting *via* the model presented below (see eqs 3 and 4). The PLE measurements were performed on the same sample (WZ InP NWs grown with V/III ratio of 350) and with the same experimental configuration as that of the spectra in Figure 3. For each excitation wavelength, the excitation power was automatically recorded, and all the PLE spectra were normalized to the exciting power as detailed in the Experimental Section. The PL measurements were recorded on the WZ InP NWs grown with a V/III ratio of 110. An ensemble of these NWs was mechanically transferred on a Si substrate in order to rule out any contribution to PL from the InP substrate, which would superimpose partly to the NW emission thus rendering PL line shape analysis troublesome. The spectra were recorded in backscattering configuration (with the direction of laser excitation and PL collection now perpendicular to the WZ $\hat{c}$ axis).

Looking at the PL data first, the intensity of the low-energy defect band (ds) decreases progressively for increasing T and only the intrinsic A peak remains visible with a character evolving from excitonic to band-to-band, as it will be shown later. Furthermore, the PL spectra broaden asymmetrically and exhibit a pronounced Boltzmann-like tail. At low temperature (<150 K), the absence of an S-shaped energy shift of transition A demonstrates the absence of localized excitons below the A peak.[44] From $T = 150$ K on, a shoulder rises about 40 meV above the emission energy of the fundamental band gap as a result of thermal population of higher energy states. That shoulder corresponds to the B transition, as apparent from the PLE spectra displayed in the same figure. In these spectra, A, B, and C transitions appear as three distinct absorption edges, preserving a well-defined step-like shape for all T's. Intense and sharp excitonic features are superimposed to the A and B absorption edges almost up to room temperature. However, the spectral resonances sizably broaden when T exceeds 150 K. An accurate determination of the critical point energies as a function of temperature is achieved by fitting the PLE line shape. In Elliot's theory, for *each* of the interband transitions i = A, B, and C with associated energy gap $E_{g,i}$, the energy ($\hbar\omega$) dependence of the absorption coefficient is given by[36,45]

$$\alpha(\hbar\omega) = \frac{4\pi e^2}{\sqrt{\varepsilon}c\omega m_0^2}|M^i_{vc}|^2\left\{\frac{1}{r^3_{exc,i}}\left[\sum_{n\geq 1}\frac{1}{n^3}A_b\left(E_{g,i} - \frac{R_i}{n^2} - \hbar\omega\right)\right] + \left(\frac{2\mu_{exc,i}}{\hbar^2}\right)^{3/2}\frac{\sqrt{R_i}}{2}\int_{E_{g,i}}^{\infty}\frac{A_b(E-\hbar\omega)}{1-\exp[-2\pi\sqrt{R_i/(E-E_{g,i})}]}dE\right\} \quad (3)$$

where ε is the static dielectric constant of the material, M^i_{vc} is the matrix element of the VB to CB transition considered (embedding the pertinent selection rules), $r_{exc,i}$ and $\mu_{exc,i}$ are the exciton radius and effective mass, respectively. $E_{g,i} - R_i/n^2 = E^i_n$ ($n = 1, 2, 3, ...$) is the energy of the n-th excited state of the free exciton relative to the i = A, B, C band gap, R_i being the exciton binding

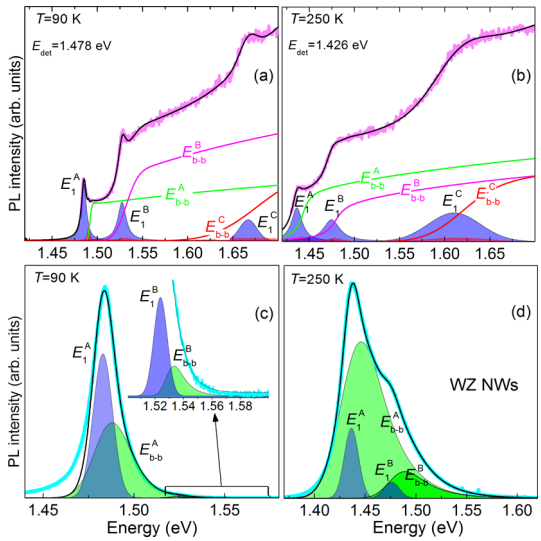

Figure 5. (a) Photoluminescence excitation (PLE) spectrum (thick magenta line) at T = 90 K of an ensemble of wurtzite InP nanowires. The PLE detection energy was set on the low-energy side of the A exciton. The black line is the best fit to the data *via* eq 3. The various contributions are indicated by filled areas for excitons E_n^i (with i = A, B, and C, and n = 1 and 2; for clarity purposes, labels E_2^A, E_2^B, and E_2^C indicating the red-colored areas are not shown) and by colored lines for continuum states E_{b-b}^i (with i = A, B, and C). We find $E_{g,A}$ = 1.492 eV, $E_{g,B}$ = 1.532 eV, and $E_{g,C}$ = 1.673 eV. (b) Same as (a) for T = 250 K with $E_{g,A}$ = 1.444 eV, $E_{g,B}$ = 1.479 eV, and $E_{g,C}$ = 1.617 eV. (c) PL spectrum (thick cyan line) at T = 90 K of an ensemble of wurtzite InP nanowires. The inset highlights the contributions of B transition to the spectrum. The various contributions to the PL spectrum are indicated using the same symbols of part (a). The black line is the best fit to the data *via* eq 4. The misfit on the low-energy side of the spectrum is due to the contribution of defect states. (d) Same as (c) for T = 250 K. Within the experimental uncertainty, the values of $E_{g,A}$ and $E_{g,B}$ found by PLE are equal to those found by PL.

energy. A_b is a suitable broadening function (Gaussian or Lorentzian) acting on the exciton and continuum states.[36] The terms within square brackets account for the exciton states. The absorption due to the continuum is reproduced by the second addend in braces, where the exponential function takes into account the Sommerfeld factor.[45] In the limit $E \gg R$ the contribution to $\alpha(\hbar\omega)$ from the continuum tends to $(E - E_g)^{1/2}$.

For exemplification purposes, Figure 5 (a,b) shows in detail a fitting of eq 3 to the PLE spectra (thick magenta lines) recorded on WZ NWs at T = 90 and 250 K, respectively. In both panels, the exciton contributions to the absorption spectra are represented by filled areas and the continuum contributions by solid lines. Specifically, resonances E_n^A, E_n^B, and E_n^C, in that order, are the contribution to the absorption of the exciton states related to transitions A, B, and C (only n = 1 and 2 states are considered). Broadened step-like functions E_{b-b}^A, E_{b-b}^B, and E_{b-b}^C represent the continuum (or band-to-band) intensities of each transition. The sum of these different contributions is shown by a thin black line. A very good agreement is obtained at these two temperatures, as well as at all other T's, as shown in Figure 4 by solid thin lines. Fit parameters are the relative amplitudes of the different contributions, the A, B, and C band gap energies $E_{g,i}$, and the full-width at half-maximum (fwhm) of the broadening functions A_b.[46] The exciton binding energy R_i is calculated in the hydrogenic effective-mass approximation for WZ crystals. We denote the exciton reduced masses parallel and perpendicular to the $\hat{c}$ axis by $\mu_{exc}^{\parallel}$ and $\mu_{exc}^{\perp}$, respectively, and the corresponding static dielectric constants by $\varepsilon_{\parallel}$ and $\varepsilon_{\perp}$. The calculated dielectric constants for WZ InP are $\varepsilon_{\perp}$ = 12.81 and $\varepsilon_{\parallel}$ = 10.44.[47] The effective mass equation for excitons in anisotropic crystals can be solved by using a linear variational method for fixed values of the anisotropy parameter defined as $\gamma = (\varepsilon_{\perp}/\varepsilon_{\parallel})\,(\mu_{exc}^{\perp}/\mu_{exc}^{\parallel})$.[48] The binding energy of the exciton ground state is then obtained in units of an effective Rydberg, $R^* = (e^4/(2\hbar^2))\,((\mu_{exc}^{\perp})/(\varepsilon_{\parallel}\varepsilon_{\perp}))$. For the A exciton we obtain γ = 0.72 and R_A =1.11 R^* = 6.4 meV by using the theoretical masses $\mu_{exc}^{\parallel}$ = 0.097 m_0 (where m_0 is the electron mass in a vacuum) and $\mu_{exc}^{\perp}$ = 0.057 m_0.[9] For the B exciton we get γ = 0.77 and R_B =1.09 R^* = 3.8 meV by using the theoretical values $\mu_{exc}^{\parallel}$ = 0.093 m_0 and $\mu_{exc}^{\perp}$ = 0.058 m_0.[9] For the C exciton, the theoretical masses $\mu_{exc}^{\parallel}$ = 0.050 m_0 and $\mu_{exc}^{\perp}$ = 0.082 m_0[9] result in γ = 2.01. We are not able to determine the corresponding R_C as $\gamma > 1$ values are not considered in ref 48. However, as the PLE spectra do not show any clear excitonic resonance for the C transition, a quantitative agreement between spectra and their respective fits can be obtained for a large range of R_C values (from 3 to 10 meV). Therefore, we used the same binding energy as the A exciton, namely R_C = 6.4 meV.

The appropriateness of the absorption model used is confirmed further by the results of Figure 5 (c,d) that show PL spectra (thick cyan lines) recorded at two different temperatures (T = 90 and 250 K) on a WZ NW sample. As already shown in Figure 4, at temperatures higher than 150 K emission due to the B transition is clearly observed on the high-energy side of the PL spectrum. The inset in Figure 5 (c) is meant to highlight the B transition contributions to the PL spectrum at lower T. In both panels (c) and (d), the thin black line is a fit of[38,49]

$$I_{PL}(\hbar\omega) = C\alpha(\hbar\omega)f(\hbar\omega;T) \qquad (4)$$

to the data, where C is a constant, $\alpha(\hbar\omega)$ is given by eq 3, and $f(\hbar\omega;T)$ is the Fermi−Dirac function accounting for the state thermal population by photoexcited carriers. In the limit of a nondegenerate semiconductor, $f(\hbar\omega;T)$ can be approximated by a Boltzmann function.[38]

In Figure 5 (c,d), excitonic and continuum contributions to the emission spectra are represented by blue and green filled areas, respectively. For PL, we only considered the n = 1 exciton states, because the higher-energy states should not contribute much and, in any case, their inclusion does not lead to major improvements to the PL fitting accuracy. The sum of these curves is shown by a thin black line in each

panel. The fits are in very good agreement with PL data at every temperature; see also thin dashed lines in Figure 4. In the least-squares fitting procedure, the free parameters are the relative amplitudes of the different contributions, the fundamental band gap energy $E_{g,A}$ (the band gaps associated with B and C transitions were determined as to maintain the energy differences with respect to $E_{g,A}$ equal to those derived from the PLE analysis), the carrier effective temperature in $f(\hbar\omega;T)$, and the fwhm of the broadening functions.[50] The exciton binding energy R_i was calculated as detailed above. The band gap energy of A determined by applying eq 4 to the PL data nearly coincide with that evaluated by PLE spectra, thus proving that the temperature variation of the energy gap can be addressed by PL spectroscopy too, provided that all the contributions to the emission spectra are duly taken into account. It is worth pointing out that the crossover in the relative intensity between the exciton and the band-to-band contributions, which occurs in the range T = 90−250 K, may hinder a determination of the thermal variation of the band gap energy from the PL peak position. This could account for the different experimental results reported in the literature, where this fitting procedure was not applied.

Polarization-Dependent PLE. We now focus on transition C. The lack of an apparent excitonic resonance in PLE spectra [see Figures 4, 5 (a,b)] makes the determination of the corresponding band gap energy a bit more complicated. To address this issue, we measured polarization-resolved PLE at different temperatures in a grazing incidence configuration, where the laser was direct perpendicular to the WZ $\hat{c}$ axis and the emitted light collected in a direction orthogonal to the laser and parallel to $\hat{c}$, as detailed in ref 31 and sketched in the inset of Figure 6 (b). For each excitation wavelength, the laser polarization was electronically switched from parallel to perpendicular with respect to the NW $\hat{c}$ axis in order to highlight specific electronic features. Indeed, the intensity of absorption in WZ-phase crystals depends on the angle formed by the polarization vector $\hat{\varepsilon}$ of absorbed photons with the NW long symmetry axis (namely, the $\hat{c}$ axis).[15,16,22,31] For parallel polarized light ($\hat{\varepsilon}\|\hat{c}$), transition C is fully allowed, B is allowed only by spin−orbit coupling, and A is forbidden. For perpendicular polarized light ($\hat{\varepsilon}\perp\hat{c}$), A and B transitions are fully allowed and C is allowed only by the spin−orbit coupling.[16,31] Therefore, we expect a greater absorption intensity for C when $\hat{\varepsilon}\|\hat{c}$. Figure 6 (a) shows T = 120 K PLE spectra recorded for two different orientations of the polarization vector with respect to the NW $\hat{c}$ axis. The detection energy was set at the A transition that, consequently, is not observed. In agreement with the above-mentioned selection rules, the PLE signal at transition B is higher for $\hat{\varepsilon}\perp\hat{c}$ than for $\hat{\varepsilon}\|\hat{c}$, and transition C is more intense for $\hat{\varepsilon}\|\hat{c}$. The energy position of the different absorption edges

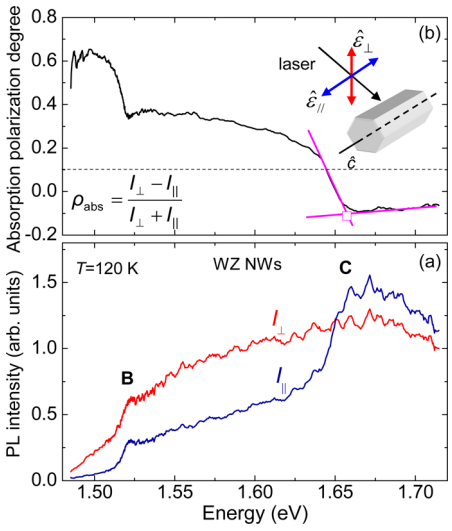

Figure 6. (a) Photoluminescence excitation (PLE) spectra of wurtzite InP nanowires at T = 120 K with detection energy set at the fundamental band gap free-exciton A. The spectra were excited with the light polarization vector parallel (blue line line, $I_{||}$) and perpendicular (red line, $I_\perp$) to the NW $\hat{c}$ axis. A sketch of the experimental configuration is shown in the top-right inset in panel (b). B and C absorption edges are indicated, the latter being clearly visible only with parallel polarized excitation. (b) Degree of linear polarization ρ_{abs} of absorbed light calculated by applying eq 5 to the two PLE spectra shown in part (a). The magenta lines highlight the graphical method employed to extract a characteristic energy (open square) for transition C.

can be more precisely obtained from the energy dependence of the absorption polarization degree

$$\rho_{abs} = \frac{I_\perp - I_{||}}{I_\perp + I_{||}} \quad (5)$$

where $I_\perp$ and $I_{||}$ are the PLE intensities for $\hat{\varepsilon}\perp\hat{c}$ and $\hat{\varepsilon}\|\hat{c}$, respectively. Figure 6 (b) shows ρ_{abs} as a function of excitation energy. Here, we do not dwell on the quantitative variation of the absorption polarization degree with energy, which is discussed in ref 31. We rather exploit ρ_{abs} as a means to deduce the variation of the C energy gap as a function of temperature. Indeed, the distinctive change of slope in $\rho_{abs}(\hbar\omega)$ observed at the C transition permits us to employ a graphical method to determine a characteristic energy to be associated with the C energy gap, as shown in Figure 6 (b) by the magenta lines.

Temperature Dependence of WZ Energy Gaps and Comparison with other Materials, Phases, and Bulk. Figure 7 (a) displays $\rho_{abs}(\hbar\omega)$ measured at different temperatures. Despite $\rho_{abs}(\hbar\omega)$ is rather noisy for T > 200 K, a well-defined change of slope can be still deduced and a characteristic energy determined (as given by open squares in the figure). Figure 7 (b) shows the energy shift with temperature of $E_{g,A}$, $E_{g,B}$, and $E_{g,C}$ (full symbols) as obtained by fitting eq 3 to the PLE spectra (see Figure 4).[51] For transition C, the energy gap values obtained by fitting eq 3 to the PLE spectra (full circles) are plotted together with those derived by the analysis

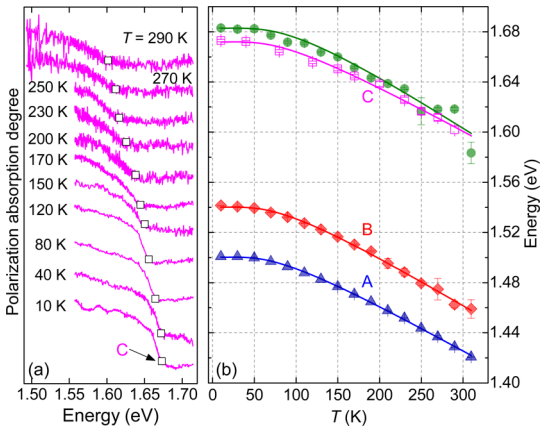

Figure 7. (a) Degree of linear polarization ρ_{abs} of absorbed light derived by polarization-resolved PLE spectra obtained from wurtzite InP nanowires at different temperatures (see Figure 6). Open squares give the characteristic energies of transition C, derived as shown in Figure 6 (b). (b) Temperature dependence of the band gap energies associated with transitions A, B, and C in wurtzite InP nanowires. For transition C, full circles refer to data extracted using a best fit to PLE spectra, and open squares refer to data extracted by employing ρ_{abs} in panel (a) and the graphical method outlined in Figure 6 (b). A and B data are determined by PLE measurements. The solid lines through the data are fittings to the data *via* eq 2, with parameter values reported in Table 1.

of the PLE polarization degree (open squares). The two sets of data match well. It is worth stressing that the two methods refer to independent sets of PLE measurements performed on different sample points and under different excitation geometries. Diamonds and triangles indicate the band-gap energy values for B and A transitions, respectively. Those data were derived by a quantitative analysis of the PLE spectra shown in Figure 4. The solid lines are a fit of eq 2 to the data, which are very well reproduced. We notice that here $(E_B - a)$ is the band gap energy at 0 K, $E_g(0)$, and not the PL peak energy.

Table 1 reports the values of the best fit parameters for A, B, and C as obtained by eq 2. For transition C, these values are tabulated for both PLE and ρ_{abs} measurements (the latter case resulting in smaller errors on the fit parameters and smaller χ^2 value). The fit parameters are similar for A, B, and C, as also apparent from Figure 7 (b), where the three energy gaps exhibit basically the same behavior. Table 1 also anticipates that the fundamental band gap energy in WZ NWs and ZB NWs (as well as bulk) shows the same thermal shrinkage.

Interestingly, the temperature dependence of all the three transitions shown in Figure 7 (b) resembles what observed in other wurtzite semiconductors, such as ZnO,[17] GaN,[40] CdS,[18] and CdSe.[41] Here, it is significant to note that WZ InP bulk is not available in nature and ours are the first measurements reporting that a same temperature dependence of A, B, and C transitions is found in small-gap WZ InP, as already found in

TABLE 1. Values of the Parameters of eq 2 As Obtained from Fits to the Experimental Data Shown in Figures 7 and 9[a]

	E_g (0) (eV)	a (meV)	θ (K)
A (WZ NWs)	1.500 ± 0.002	45 ± 2	238 ± 9
B (WZ NWs)	1.540 ± 0.005	50 ± 5	250 ± 20
C (WZ NWs) ρ_{abs}	1.672 ± 0.013	49 ± 12	258 ± 40
C (WZ NWs)	1.680 ± 0.020	64 ± 30	290 ± 80
ZB NWs	1.423 ± 0.003	50 ± 4	260 ± 10
ZB bulk	1.422 ± 0.002	54 ± 2	265 ± 7

[a] E_g (0) is the band gap energy at 0 K. a and $k_B\theta$ can be regarded as phenomenological quantities associated to the strength of the electron−phonon interaction and to an average phonon energy, respectively.

wide band gap nitride III−V (*e.g.*, GaN) and II−VI (*e.g.*, ZnO, CdS, and CdSe) compounds with WZ phase. This is, therefore, a *general feature* of WZ materials, in NW or bulk forms (of course, different materials exhibit a quantitatively different extent of the band gap reduction with T). Additionally, it was found that the A, B, and C energy gaps in WZ GaN[52] and AlGaN[53] display a different thermal shrinkage whenever a residual in-plane biaxial stress develops between the deposited layer and the substrate.[54] This indicates that our WZ InP NWs grown on ZB InP (111) substrate are actually strain-free, a material property that we can infer from an all-optical sample characterization.

In order to verify if the specific NW morphology influences the thermal red-shift of the interband transition energies, we compared the temperature dependence of E_g measured in zincblende InP NWs with that measured in an InP bulk reference. Figure 8 shows the PL spectrum (thick cyan lines) of ZB InP NWs (mechanically transferred on a Si substrate) and that of an InP epilayer, both recorded at $T = 290$ K. A fitting *via* eq 4 is also displayed along with the contribution of exciton and continuum states. At high T, the relative contribution of exciton states with respect to that of continuum states is smaller in NWs than that in the bulk. The increased exciton ionizability in NWs is likely due to a higher density of surface states and/or crystallographic defects than in bulk. Interestingly, those data show that the assignment of the true band gap energy to the PL peak can be misleading. In fact, ZB InP bulk and ZB NWs have the same energy gap (shown by the double arrow in the figure), as it is found by an analysis of the PL spectra using eq 4. Nevertheless, the PL peak position is different in the two cases due to a different weight of the continuum states.

Figure 9 displays the relative shift of E_g as a function of temperature in ZB InP NWs (diamonds) and InP bulk (triangles). The triangles are downward shifted by 10 meV for clarity purposes. In both samples, the band gap energy was derived from PL measurements, as those shown in Figure 8, after fitting the data *via* eq 4. Data for $T = 10$ and 30 K, where a reliable line shape fitting could not be obtained because of the presence

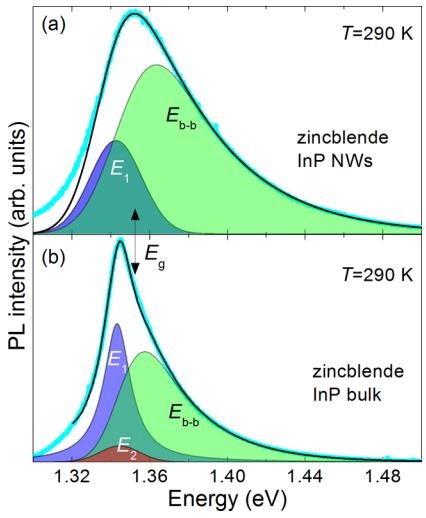

Figure 8. (a) Photoluminescence (PL) spectra (thick cyan line) of an ensemble of zincblende InP nanowires at T = 290 K. The thin black line is a fit to the PL data *via* eq 4. The exciton ground state (E_1) and continuum (E_{b-b}) contributions are displayed as blue and green filled areas, respectively. The misfit on the low-energy side is due to the contribution of defect states. (b) Same as (a) for zincblende bulk InP (the E_2 exciton state is also present). Notice that a same band gap energy results from the fit procedure, as indicated by the double arrow, in spite of the different PL peak energies.

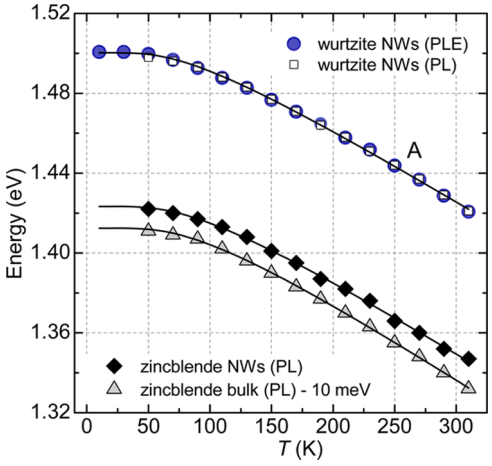

Figure 9. Temperature dependence of the fundamental band gap energy ($E_{g,A}$) of WZ InP NWs derived by photoluminescence (small open squares) and photoluminescence excitation [large full circles; same data as Figure 7 (b)] measurements. Diamonds and triangles show the band gap energies for zincblende InP nanowires and InP bulk, respectively. The triangles are downward shifted by 10 meV for clarity purposes. The solid lines are a fit of eq 2 to the data with the parameter values reported in Table 1.

of defect states, are missing. The T dependence of both samples is very close and similar to the results found in WZ InP NWs, whose fundamental energy gap ($E_{g,A}$) is shown in the same figure by full large circles (PLE data) and open small squares (PL data) that match each other very well, thus proving the robustness of our analysis. The present result contrasts markedly with the previous finding of a different thermal shrinkage of the band gap energies of WZ and ZB InP NWs.[6] Our results also contrast with what found by the authors reporting that the thermal shift of the fundamental band gap energy in WZ GaAs NWs differs sizably with respect to that measured in bulk GaAs. According to those authors, this would support a Γ_8^C character for the CB minimum in WZ GaAs.[20] Moreover, our results differ from resonant Raman scattering measurements performed on WZ GaAs NWs indicating that the T-induced redshift of transition C is greater than that of the band gap in ZB GaAs.[39]

Our findings clearly show that the main mechanisms ruling the extent of the band gap variation with temperature, namely, the lattice expansion and the electron−phonon interaction, do not depend on the NW crystal phase. Indeed, in both ZB and WZ phases of a binary compound, which we can indicate as AB, four A atoms nearest neighbors of a B atom are placed at the vertices of a regular tetrahedron around the B atom and nine out of the 12 second nearest neighbors are at identical crystallographic locations while the other second nearest neighbors are equidistant.[9] Owing to these similar lattice characteristics, the crystal deformation potentials are expected to be comparable in WZ and ZB. In turn, this should result in a similar lattice thermal expansion. Moreover, it is also reasonable to expect a rather similar electron−phonon interaction in WZ and ZB crystals due to their similar phonon dispersion curves.[55,56] This is consistent with preceding theoretical and experimental works highlighting the absence of a major role played by the crystal phase in determining some relevant thermal properties of NWs, such as specific heat, thermal energy group velocity, and phonon−phonon interactions.[55,57]

CONCLUSIONS

We presented a detailed study of the A, B, and C band gap energies in WZ InP nanowires from 10 K to room temperature. Efficient absorption and emission was observed at all temperatures, an important feature in an application perspective. PLE and PL measurements combined with a theoretical line shape analysis permitted us to establish that in WZ InP the A, B, and C band gaps undergo a same decrease with increasing temperature. This finding highlights a general feature of the thermal properties of WZ materials holding regardless of the bond polarity and energy gap of the crystal. Indeed, a same reduction of the A, B, and C energies upon temperature increase is found also in hexagonal GaN,[40] ZnO,[17] CdS[18] and CdSe[41] bulk materials. Furthermore, comparative studies of the temperature dependence of the band gap performed on ZB InP NWs and bulk InP permitted us to highlight a negligible role played by the WZ/ZB crystal phase difference in determining the deformation potentials and the electron−phonon interaction in the lattice. On this ground, important quantities related to heat transfer and dissipation in the lattice of nanowires

are expected to be independent of the NW crystal phase. This is of relevance, for instance, in discriminating which structural characteristics of these nanostructures matter most in the reduced thermal conductivity usually exploited in NW-based thermoelectric devices.[55,57]

EXPERIMENTAL SECTION

The nanowires were grown by Au-catalyzed metal−organic chemical-vapor deposition (MOCVD) following the vapor−liquid−solid mechanism. The diameter of the Au nanoparticles was 30 nm, and the precursors were trimethylindium (TMIn) and phosphine (PH_3). We investigated two samples of InP NWs with the wurtzite structure, both fabricated on semi-insulating InP (111)B substrates. One sample was grown at the temperature of 480 °C with V/III ratio of 350, the other one was grown at the same temperature with V/III ratio of 110. The two samples have very similar structural and optical properties. InP NWs with the zincblende phase were grown by MOCVD on a semi-insulating InP (100) substrate. Growth temperature and V/III ratio were 450 °C and 350, respectively. The crystal structure of all the NW samples was investigated using a Jeol 2100F transmission electron microscopy operated at 200 kV. An InP bulk sample was also used for comparison purposes. It is a 3 μm-thick (100) epilayer grown by MOCVD at 650 °C.

PL and PLE measurements on NW ensembles were performed at different temperatures in a He closed-cycle cryostat. PL was excited by a frequency-doubled Nd:YVO_4 laser with a spot diameter of ∼200 μm, dispersed by a 0.75 m monochromator, and detected by a liquid N-cooled Si CCD. All PL spectra were normalized by the setup response. PLE measurements were performed by using a continuous-wave Ti:sapphire tunable laser as excitation source (λ_{exc} = 880−700 nm). The PLE signal was dispersed by a 1.5 m double monochromator equipped with 600 grooves/mm gratings and detected by a Peltier-cooled GaAs photomultiplier (detection bandwidth of 0.2 meV). For each λ_{exc}, the wavelength and power (P) of the scanning laser were automatically measured by a Michelson interferometer (resolution of 0.02 nm) and a calibrated Si power meter, respectively. P could not be maintained constant in a same PLE spectrum due to the wavelength dependence of the reflectivity of the mirrors in the Ti:sapphire laser. P varied by a factor of ∼3 in the 1.40−1.70 eV energy range. Moreover, at a given λ_{exc}, power was raised by a factor of about 10 between 10 and 310 K to compensate for signal losses due to the increasing role played by nonradiative recombination. Therefore, all the PLE spectra shown in the paper were duly normalized by P^{α}. The value of the exponent α at given temperatures was evaluated from the experimental PL intensity dependence on the excitation power at the detection energy of the corresponding PLE spectrum. The exponent α was found to vary from ∼1.5 to ∼1.2 when the temperature was increased from 10 to 310 K.

The polarization-resolved PLE measurements in a grazing incidence configuration were performed with the laser direct perpendicular to the WZ $\hat{c}$ axis and the emitted light collected in a direction orthogonal to the laser (and parallel to $\hat{c}$). A liquid crystal variable retarder, set at $\lambda/2$ retardance, was inserted in the exciting beam path in order to switch electronically between laser polarizations parallel and perpendicular with respect to the NW $\hat{c}$ axis, while keeping the excitation wavelength and power fixed.

Conflict of Interest: The authors declare no competing financial interest.

Acknowledgment. M.D.L., M.C., and A.P. acknowledge funding by Sapienza Università di Roma under the "Avvio alla Ricerca 2014", "Ateneo 2012", and "Ateneo 2013" grants, in that order. The Australian authors acknowledge the Australian Research Council for financial support and Australian National Fabrication Facility and Australian Microscopy and Microanalysis Research Facility for providing access to some of the equipment used in this work.

REFERENCES AND NOTES

1. Dasgupta, N. P.; Sun, J.; Liu, C.; Brittman, S.; Andrews, S. C.; Lim, J.; Gao, H.; Yan, R.; Yang, P. 25th Anniversary Article: Semiconductor Nanowires—Synthesis, Characterization, and Applications. *Adv. Mater.* **2014**, *26*, 2137–2184.
2. Caroff, P.; Bolinsson, J.; Johansson, J. Crystal Phases in III−V Nanowires: From Random Toward Engineered Polytypism. *IEEE J. Sel. Top. Quantum Electron.* **2011**, *17*, 829–846.
3. Lehmann, S.; Wallentin, J.; Jacobsson, D.; Deppert, K.; Dick, K. A. A General Approach for Sharp Crystal Phase Switching in InAs, GaAs, InP, and GaP Nanowires Using Only Group V Flow. *Nano Lett.* **2013**, *13*, 4099–4105.
4. Akopian, N.; Patriarche, G.; Liu, L.; Harmand, J.-C.; Zwiller, V. Crystal Phase Quantum Dots. *Nano Lett.* **2010**, *10*, 1198–1201.
5. Yeh, C.-Y.; Wei, S. H.; Zunger, A. Relationships Between the Band Gaps of the Zinc-blende and Wurtzite Modifications of Semiconductors. *Phys. Rev. B: Condens. Matter Mater. Phys.* **1994**, *50*, 2715–2718.
6. Mishra, A.; Titova, L. V.; Hoang, T. B.; Jackson, H. E.; Smith, L. M.; Yarrison-Rice, J. M.; Kim, Y.; Joyce, H. J.; Gao, Q.; Tan, H. H.; *et al.* Polarization and Temperature Dependence of Photoluminescence from Zincblende and Wurtzite InP Nanowires. *Appl. Phys. Lett.* **2007**, *91*, 263104.
7. De Luca, M.; Lavenuta, G.; Polimeni, A.; Rubini, S.; Grillo, V.; Mura, F.; Miriametro, A.; Capizzi, M.; Martelli, F. Excitonic Recombination and Absorption in $In_xGa_{1-x}As$/GaAs Heterostructure Nanowires. *Phys. Rev. B: Condens. Matter Mater. Phys.* **2013**, *87*, 235304.
8. Assali, S.; Zardo, I.; Plissard, S.; Kriegner, D.; Verheijen, M. A.; Bauer, G.; Meijerink, A.; Belabbes, A.; Bechstedt, F.; Haverkort; *et al.* Direct Band Gap Wurtzite Gallium Phosphide Nanowires. *Nano Lett.* **2013**, *13*, 1559–1563.
9. De, A.; Pryor, C. E. Predicted Band Structures of III-V Semiconductors in the Wurtzite Phase. *Phys. Rev. B: Condens. Matter Mater. Phys.* **2010**, *81*, 155210.
10. Cheiwchanchamnangij, T.; Lambrecht, W. R. L. Band Structure Parameters of Wurtzite and Zinc-Blende GaAs under Strain in the GW Approximation. *Phys. Rev. B: Condens. Matter Mater. Phys.* **2011**, *84*, 035203.
11. Bechstedt, F.; Belabbes, A. Structure, Energetics, and Electronic States of III−V Compound Polytypes. *J. Phys.: Condens. Matter* **2013**, *25*, 273201and references therein.
12. Dacal, L. C. O.; Cantarero, A. *Ab Initio* Electronic Band Structure Calculation of InP in the Wurtzite Phase. *Solid State Commun.* **2011**, *151*, 781–784.
13. De Luca, M.; Polimeni, A.; Capizzi, M.; Meaney, A. J.; Christianen, P. C. M.; Maan, J. C.; Mura, F.; Rubini, S.; Martelli, F. Determination of Exciton Reduced Mass and Gyromagnetic Factor of Wurtzite (InGa)As Nanowires by Photoluminescence Spectroscopy under High Magnetic Fields. *ACS Nano* **2013**, *7*, 10717–10725.
14. De Luca, M.; Polimeni, A.; Fonseka, H. A.; Meaney, A. J.; Christianen, P. C. M.; Maan, J. C.; Paiman, S.; Tan, H. H.; Jagadish, C.; Capizzi, M. Magneto-Optical Properties of Wurtzite-Phase InP Nanowires. *Nano Lett.* **2014**, *14*, 4250–4256.
15. Birman, J. L. Some Selection Rules for Band-Band Transitions in Wurtzite Structure. *Phys. Rev.* **1959**, *114*, 1490–1492.
16. Tronc, P.; Kitaev, Y. E.; Wang, G.; Limonov, M. F.; Panfilov, A. G.; Neu, G. Optical Selection Rules for Hexagonal GaN. *Phys. Status Solidi B* **1999**, *216*, 599–603.
17. Alawadhi, H.; Tsoi, S.; Lu, X.; Ramdas, A. K.; Grimsditch, M.; Cardona, M.; Lauck, R. Effect of Temperature on Isotopic Mass Dependence of Excitonic Band Gaps in Semiconductors: ZnO. *Phys. Rev. B: Condens. Matter Mater. Phys.* **2007**, *75*, 205207.

18. Imada, A.; Ozaki, S.; Adachi, S. Photoreflectance Spectroscopy of Wurtzite CdS. *J. Appl. Phys.* **2002**, *92*, 1793–1798.
19. Cardona, M. Renormalization of the Optical Response of Semiconductors by Electron-Phonon Interaction. *Phys. Status Solidi A* **2001**, *188*, 1209–1232.
20. Ahtapodov, L.; Todorovic, J.; Olk, P.; Mjåland, T.; Slåttnes, P.; Dheeraj, D. L.; van Helvoort, A. T.; Fimland, B.-O.; Weman, H. A Story Told by a Single Nanowire: Optical Properties of Wurtzite GaAs. *Nano Lett.* **2012**, *12*, 6090–6095.
21. Kim, D. C.; Dheeraj, D. L.; Fimland, B. O.; Weman, H. Polarization Dependent Photocurrent Spectroscopy of Single Wurtzite GaAs/AlGaAs Core-Shell Nanowires. *Appl. Phys. Lett.* **2013**, *102*, 142107.
22. Gadret, E. G.; Dias, G. O.; Dacal, L. C. O.; de Lima, M. M., Jr.; Ruffo, C. V. R. S.; Iikawa, F.; Brasil, M. J. S. P.; Chiaramonte, T.; Cotta, M. A.; Tizei, L. H. G.; *et al.* Valence-Band Splitting Energies in Wurtzite InP Nanowires: Photoluminescence Spectroscopy and *Ab Initio* Calculations. *Phys. Rev. B: Condens. Matter Mater. Phys.* **2010**, *82*, 125327.
23. Perera, S.; Pemasiri, K.; Fickenscher, M. A.; Jackson, H. E.; Smith, L. M.; Yarrison-Rice, J.; Paiman, S.; Gao, Q.; Tan, H. H.; *et al.* Probing Valence Band Structure in Wurtzite InP Nanowires Using Excitation Spectroscopy. *Appl. Phys. Lett.* **2010**, *97*, 023106.
24. Tuin, G. L.; Borgström, M. T.; Tragårdh, J.; Ek, M.; Wallenberg, L. R.; Samuelson, L.; Pistol, M. Valence Band Splitting in Wurtzite InP Nanowires Observed by Photoluminescence and Photoluminescence Excitation Spectroscopy. *Nano Res.* **2011**, *4*, 159–163.
25. Montazeri, M.; Wade, A.; Fickenscher, M.; Jackson, H. E.; Smith, L. M.; Yarrison-Rice, J. M.; Gao, Q.; Tan, H. H.; Jagadish, C. Photomodulated Rayleigh Scattering of Single Semiconductor Nanowires: Probing Electronic Band Structure. *Nano Lett.* **2011**, *11*, 4329–4336.
26. Alouane, M. H. H.; Chauvin, N.; Khmissi, H.; Naji, K.; Ilahi, B.; Maaref, H.; Patriarche, G.; Gendry, M.; Bru-Chevallier, C.; Excitonic, C. Properties of Wurtzite InP Nanowires Grown on Silicon Substrate. *Nanotechnology* **2013**, *24*, 035704.
27. Perera, S.; Shi, T.; Fickenscher, M. A.; Jackson, H. E.; Smith, L. M.; Yarrison-Rice, J. M.; Paiman, S.; Gao, Q.; Tan, H. H.; Jagadish, C. Illuminating the Second Conduction Band and Spin−Orbit Energy in Single Wurtzite InP Nanowires. *Nano Lett.* **2013**, *13*, 5367–5372.
28. Li, K.; Sun, H.; Ren, F.; Ng, K. W.; Tran, T.-T. D.; Chen, R.; Chang-Hasnain, C. J. Tailoring the Optical Characteristics of Microsized InP Nanoneedles Directly Grown on Silicon. *Nano Lett.* **2014**, *14*, 183–190.
29. Gao, Q.; Saxena, D.; Wang, F.; Fu, L.; Mokkapati, S.; Guo, Y.; Li, L.; Wong-Leung, J.; Caroff, P.; Tan, H. H.; *et al.* Selective-Area Epitaxy of Pure Wurtzite InP Nanowires: High Quantum Efficiency and Room-Temperature Lasing. *Nano Lett.* **2014**, *14*, 5206–5211.
30. Vu, T. T. T.; Zehender, T.; Verheijen, M. A.; Plissard, S. R.; Immink, G. W. G.; Haverkort, J. E. M.; Bakkers, E. P. A. M. High Optical Quality Single Crystal Phase Wurtzite and Zincblende InP Nanowires. *Nanotechnology* **2013**, *24*, 115705.
31. De Luca, M.; Zilli, A.; Fonseka, H. A.; Mokkapati, S.; Miriametro, A.; Tan, H. H.; Smith, L. M.; Jagadish, C.; Capizzi, M.; Polimeni, A. Polarized Light Absorption in Wurtzite InP Nanowire Ensembles. *Nano Lett.* **2015**, *15*, 998–1005.
32. Viña, L.; Logothetidis, S.; Cardona, M. Temperature Dependence of the Dielectric Function of Germanium. *Phys. Rev. B: Condens. Matter Mater. Phys.* **1984**, *30*, 1979–1991.
33. Lautenschlager, P.; Garriga, M.; Cardona, M. Temperature Dependence of the Interband Critical-Point Parameters of InP. *Phys. Rev. B: Condens. Matter Mater. Phys.* **1987**, *36*, 4813–4820.
34. Murotani, H.; Yamada, Y.; Tabata, T.; Honda, Y.; Yamaguchi, M.; Amano, H. Effects of Exciton Localization on Internal Quantum Efficiency of InGaN Nanowires. *J. Appl. Phys.* **2013**, *114*, 153506.
35. Polimeni, A.; Capizzi, M.; Geddo, M.; Fischer, M.; Reinhardt, M.; Forchel, A. Effect of Nitrogen on the Temperature Dependence of the Energy Gap in $In_xGa_{1-x}As_{1-y}N_y$/GaAs Single Quantum Wells. *Phys. Rev. B: Condens. Matter Mater. Phys.* **2001**, *63*, 195320.
36. Grilli, E.; Guzzi, M.; Zamboni, R.; Pavesi, L. High-Precision Determination of the Temperature Dependence of the Fundamental Energy Gap in Gallium Arsenide. *Phys. Rev. B: Condens. Matter Mater. Phys.* **1992**, *45*, 1638–1644.
37. Polimeni, A.; Patanè, A.; Grassi Alessi, M.; Capizzi, M.; Martelli, F.; Bosacchi, A.; Franchi, S. Stokes Shift in Quantum Wells: Trapping *versus* Thermalization. *Phys. Rev. B: Condens. Matter Mater. Phys.* **1996**, *54*, 16389–16392.
38. Gurioli, M.; Vinattieri, A.; Martinez-Pastor, J.; Colocci, M. Exciton Thermalization in Quantum-Well Structures. *Phys. Rev. B: Condens. Matter Mater. Phys.* **1994**, *50*, 11817–11826.
39. Ketterer, B.; Heiss, M.; Livrozet, M. J.; Rudolph, A.; Reiger, E.; Fontcuberta i Morral, A. Determination of the Band Gap and the Split-Off Band in Wurtzite GaAs using Raman and Photoluminescence Excitation Spectroscopy. *Phys. Rev. B: Condens. Matter Mater. Phys.* **2011**, *83*, 125307.
40. Shan, W.; Schmidt, T.; Yang, X.; Hwang, S.; Song, J.; Goldenberg, B. Temperature Dependence of Interband Transitions in GaN Grown by Metalorganic Chemical Vapor Deposition. *Appl. Phys. Lett.* **1995**, *66*, 985–987.
41. Logothetidis, S.; Cardona, M.; Lautenschlager, P.; Garriga, M. Temperature Dependence of the Dielectric Function and the Interband Critical Points of CdSe. *Phys. Rev. B: Condens. Matter Mater. Phys.* **1986**, *34*, 2458–2469.
42. Fonseka, H. A.; Caroff, P.; Wong-Leung, J.; Ameruddin, A. S.; Tan, H. H.; Jagadish, C. Nanowires Grown on InP (100): Growth Directions, Facets, Crystal Structures, and Relative Yield Control. *ACS Nano* **2014**, *8*, 6945–6954.
43. Yu, P. Y.; Cardona, M. *Fundamentals of Semiconductors*, 3rd ed.; Springer: Berlin, 2005; Chapter 7, p 369.
44. Polimeni, A.; Capizzi, M.; Geddo, M.; Fischer, M.; Reinhardt, M.; Forchel, A. Effect of Temperature on the Optical Properties of (InGa)(AsN)/GaAs Single Quantum Wells. *Appl. Phys. Lett.* **2000**, *77*, 2870–2872.
45. Elliot, R. J. Intensity of Optical Absorption by Excitons. *Phys. Rev.* **1957**, *108*, 1384–1389.
46. We employed Lorentzian broadening functions for A and B transitions, and a Gaussian function for transition C. These choices gave us the best agreement between the data and the model.
47. De, A.; Pryor, C. E. Optical Dielectric Functions of Wurtzite III-V Semiconductors. *Phys. Rev. B: Condens. Matter Mater. Phys.* **2012**, *85*, 125201.
48. Baldereschi, A.; Diaz, M. G. Anisotropy of Excitons in Semiconductors. *Il Nuovo Cimento* **1970**, *68 B*, 217–229.
49. Pankove, J. *Optical Processes in Semiconductors*; Dover Publications: Mineola, NY, 1971.
50. We arbitrarily employed Lorentzian or Gaussian functions depending on the quality of the resulting fit.
51. We point out that values of the exciton binding energies slightly smaller/larger than the ones used in the fittings would only red/blueshift the energy gap of transitions A, B, and C slightly (<0.5 meV), regardless of temperature.
52. Li, C. F.; Huang, Y. S.; Malikova, L.; Pollak, F. H. Temperature Dependence of the Energies and Broadening Parameters of the Interband Excitonic Transitions in Wurtzite GaN. *Phys. Rev. B: Condens. Matter Mater. Phys.* **1996**, *55*, 9251–9254.
53. Malikova, L.; Huang, Y. S.; Pollak, F. H.; Feng, Z. C.; Schurmanb, M.; Stall, R. A. Temperature Dependence of the Energies and Broadening Parameters of the Excitonic Interband Transitions in $Ga_{0.95}Al_{0.05}N$. *Solid State Commun.* **1977**, *103*, 273–278.
54. Gil, B.; Briot, O.; Aulombard, R.-L. Valence-band Physics and the Optical Properties of GaN Epilayers Grown onto Sapphire with Wurtzite Symmetry. *Phys. Rev. B: Condens. Matter Mater. Phys.* **1995**, *52*, 17028–17031.
55. Mukhopadhyay, S.; Stewart, D. A. First-Principles Study of the Phonon Dispersion and Dielectric Properties of Wurtzite InP: Role of In *4d* Electrons. *Phys. Rev. B: Condens. Matter Mater. Phys.* **2014**, *89*, 054302.

56. Gadret, E. G.; de Lima, M. M., Jr.; Madureira, J. R.; Chiaramonte, T.; Cotta, M. A.; Iikawa, F.; Cantarero, A. Optical Phonon Modes of Wurtzite InP. *Appl. Phys. Lett.* **2013**, *102*, 122101.
57. Zhou, F.; Moore, A. L.; Bolinsson, J.; Persson, A.; Fröberg, L.; Pettes, M. T.; Kong, H.; Rabenberg, L.; Caroff, P.; Stewart, D. A.; *et al.* Thermal Conductivity of Indium Arsenide Nanowires with Wurtzite and Zinc Blende Phases. *Phys. Rev. B: Condens. Matter Mater. Phys.* **2011**, *83*, 205416.